An Inquiry into the Synthesis of Zinc/Chelidonate-based MOFs and Their Potential Uses in the Prevention of Hernia Mesh Infections

Student PI:

Ryan Vassalotti

Undergraduate Biology Student

Biology Department

Florida Southern College

111 Lake Hollingsworth Dr.

Lakeland, FL 33801

Email: vassryan@aol.com

Co-Principal Investigators:

Jarrod F. Eubank, Ph. D

Associate Professor of Chemistry

Department of Chemistry

Florida Southern College

111 Lake Hollingsworth Dr.

Lakeland, FL 33801

Phone: (863) 680-4199

Email: jeubank@flsouthern.edu

Table of Contents

A. Abstract

A hernia is one of the most common medical issues that occurs in the entire world, affecting millions of people yearly. As part of the surgery to repair a hernia, the physician will often insert a mesh material to prevent recurrence of the hernia. Despite their high efficacy in preventing recurrence of the hernia, these hernia meshes are unfortunately prone to infection. Hernia mesh infections affect thousands of people every year and cost the individuals large amounts of unnecessary time and money. The field of metal-organic frameworks (MOFs) has opened up a promising path towards solving this issue. The successful synthesis of antimicrobial MOFs and biocompatible MOFs demonstrates that there is merit in pursuing biomedical applications. With the help of antimicrobial materials like MOFs it may be possible to prevent these postoperative infections. Synthesis of a Zn-based analogue to a previously characterized antimicrobial Cu-basedMOF, me137, was successful. The results of this study indicate that control of both morphology and structure in Zn-based MOFs is possible. Additionally, the Zn-based MOFs appear to be more chemically stable than similar Cu-based MOFs. Antimicrobial assays have demonstrated that the Zn-based MOFs are capable of inhibiting the growth of *E. coli* and *S. aureus*. Early adhesion tests have shown that growth of Compound 1 (RV22) onto unmodified polypropylene is not an interaction that readily occurs. Thus, methods for modifying polypropylene to take on a form more conducive to MOF adhesion was investigated. A method for oxidizing polypropylene with the use of $KMnO_4$, NaOH, and heat was found to be successful, but adhesion of Compound 1 onto the oxidized polypropylene has not yet been achieved.

B.1 Introduction

Previous research has also shown that nearly 27% of men and 3% of women will acquire inguinal hernias.[1] Hernias must be repaired surgically and often involve the use of hernia meshes. These meshes keep all of the repaired muscle together and prevent recurrence of the hernia. Although hernia meshes are useful in preventing the hernia from recurring, they are unfortunately prone to infection. Postoperative hernia mesh infection is a common and widespread medical issue. Prior to laparoscopic surgery, mesh infections were higher than they are today. In spite of this, mesh infections still occur at rates as high as 10% in individuals given polytetrafluoroethylene (PTFE) meshes.[2] Although treatment of these infections is possible, it is often expensive, time-consuming, and potentially dangerous. Of the individuals that undergo open inguinal hernia repair surgery, as high as 9-18% of individuals will experience postoperative mesh infections.[2] These infections are often caused by bacteria such as *S. aureus*, *E. coli*, *Enterococci*, and some *Staphylococcus* species. It is more cost-effective and safe to prevent the mesh infections from occurring rather than treating them afterwards.[2] There is a need to develop better materials or strategies to combat these infections.

One unique set of materials known as MOFs, are well-poised to address these challenges. To potentially/help prevent these infections, this study aims to synthesize particular MOFs with antimicrobial properties. MOFs possess great potential for solving the issue of postoperative hernia mesh infections. MOFs are materials that consist of a positively-charged metal ion(s) and organic ligands. MOFs can adopt 1-periodic, 2-periodic, or 3-periodic, and even stable porous, structures depending on the organic ligands, the molecular geometry of the metal, the solvent system, and reaction conditions. These MOFs have been the subject of significant investigation in recent years and have been studied for their uses in storage (including storage of drug

molecules), catalysis, sensing, and purification.[3,4,5,6] A potential use of MOFs that is the interest of this study is use as an antimicrobial agent. Copper, cobalt, silver,[7,8] and zinc-based MOFs[9] have all been shown to exhibit antimicrobial properties. The mechanisms of the antimicrobial action vary and are overall not well-understood, so it is difficult to predict if a MOF will be antimicrobial merely based on its structure.

MOFs are capable of adopting a variety of morphologies and exhibiting properties unique to both organic and inorganic compounds. The versatility of MOFs makes them promising candidate materials for biomedical application. For instance, the metal ions (e.g.: Zn, Cu, Co, Ag) have been shown to demonstrate antimicrobial properties when part of a MOF.[1,2,3] The organic ligand used in this project, chelidonic acid, has also shown promise as an antimicrobial agent.[4] Previous research has also demonstrated that synthesis of Cu- and Zn-based MOFs with chelidonate (CDO) ligands is possible.[10,11] However, no current research has specifically applied MOFs to hernia meshes.

Addition of antimicrobial ligands can improve the chance that the resulting MOF will exhibit antimicrobial properties. Once consistent synthesis of a particular MOF structure is attained, it will be possible to exchange some of the ligands (e.g. pyridine) with molecules known to have antimicrobial effects (e.g., sulfa drugs, β-lactam ring, etc.). One such molecule, guaiacol, has already been shown to be capable of being encapsulated by a Cu-based MOF, HKUST-1.[12] Alternatively, the MOF could be used to store and transport antibiotics or other drug molecules within its porous structure.

Thus, the intent of this project will be to synthesize Zn-based MOFs with antimicrobial properties and explore potential for adhering them to hernia mesh materials. The research focused on reproducible synthesis of Zn-based MOFs. Two such MOFs, Compound 1 (RV22)

and Compound 2 (RV9.16 photo product) (see Results), were produced and the effects of exposing these MOFs to various strains of bacteria associated with postoperative hernia mesh infections. Unpublished results from the lab indicate that the combined antimicrobial properties of the MOF produce a synergistic effect that results in more potent antimicrobial function than either of the parts. This synergism was partially confirmed by comparing the zones of inhibition produced by chelidonic acid, zinc, and the Zn-based MOFs. The mechanism of antimicrobial action was investigated; preliminary results suggested the mechanism was bacteriostatic. In addition, growth of Compound 1 onto polypropylene was attempted. Unmodified polypropylene did not allow for MOF growth, so a method of oxidizing polypropylene to poly(acrylic acid) via potassium permanganate was explored. This method was inspired by a previous study that utilized ammonium permanganate to convert polypropylene to poly(acrylic acid).[13] This method appeared to successfully produce poly(acrylic acid), but experiments have not yet revealed whether or not Compound 1 can grow on this newly synthesized poly(acrylic acid).

B.1.1 Metal-Organic Framework (MOF) Synthesis

Before antimicrobial activity can be studied, reliable synthesis of the MOF must be attained. In addition, due to the high standards required of biomedical materials, synthesis should be both efficacious and yield minimal byproducts. The general protocol being used for synthesizing the zinc-based MOF is microscale solvothermal synthesis. This involves first adding the desired organic ligand(s) and metal to the reaction vial. Then, the solvents can be added and the mixture can be heated at a specific temperature for a predetermined length of time.

There are numerous design and synthesis strategies for MOFs. Each factor involved in the reaction can be altered, and each can result in changes to morphology, size, and/or structure.

The difference between morphology and structure is important to delineate. Morphology refers to the shape of the actual crystals produced while structure refers to the framework composition.[14]

The structure of Compound 1 is shown in Figure 1. The unit cell of Compound 1 is trigonal bipyramidal with two chelidonic bridging ligands oriented in-line with the y/z-axis, two pyridine terminal ligands oriented in-line with the x-axis, and one water molecule oriented approximately with the z-axis. With a 1-periodic MOF (like the one in this study), the metals and ligands form linear polymeric chains that can stack together and interact with each other via π-π stacking and hydrogen bonding. For the specific structure in this study, Compound 1, chains that are adjacent to each with respect to the x-axis can demonstrate pyridine antiparallel overlapping with minimal offset. The pyridines in these adjacent chains exist 3.435 Å apart, which allows for the π-π stacking interaction (Figure 1 (Left)).[11] The chains that are adjacent with respect to the x-axis also show overlapping chelidonate ligands. These ligands exist a distance of 3.585 Å apart, which is also within the accepted range to facilitate π-π stacking (Figure 1 (Right)). Like with the pyridines, the chelidonates demonstrate minimal offset. The carbonyls of chelidonate ligands hydrogen bond with water molecules of chains that are adjacent with respect to the y/z-axis (Figure 1 (Middle)).

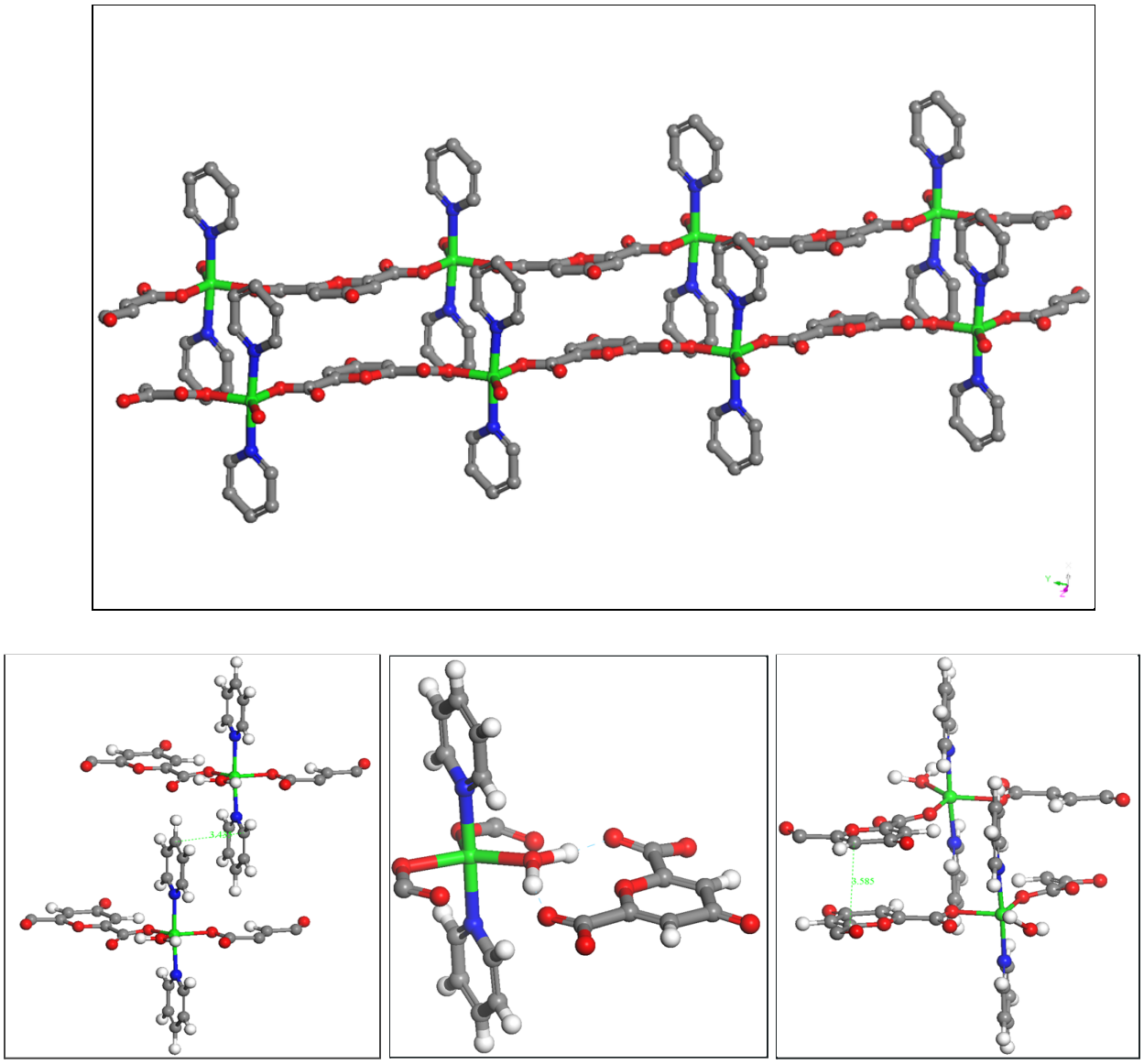

Figure 1. Crystal structure of Compound 1 $[(Zn(C_7H_2O)(H_2O)(C_5H_5N)_2)]_n$. Top - Image of two repeating chains of Compound 1. Left - This image highlights the π-π stacking between the pyridines (nitrogens shown in blue). Middle - A different view highlighting the hydrogen bonding between the different chains. Right- This image highlights the π-π stacking between chelidonates on adjacent MOF chains.

For the purposes of single crystal analysis, crystal morphology should possess the general properties of being clear, relatively large, and isolated (not nucleated), whereas for some applications, like biomedical, the crystal morphology should be more powdery and small to

increase surface area and allow for greater contact between the pathogen and the antimicrobial components of the MOF.

B.1.2 Antimicrobial MOFs and their Biocompatibility

Regardless of the presence or absence of antimicrobial properties, a MOF designed for biomedical use must be biocompatible. Copper-based MOFs, like the prototypical HKUST-1, have been shown to demonstrate antimicrobial properties, but they are also toxic to humans in high enough doses.[7] Zinc-based MOFs, on the other hand, are found to be largely nontoxic to humans.[15] The main reason for this is that zinc is a bioactive ion, meaning it has a biological function. Metal ions and their allowed amounts in the human body are shown in Table 1. The results in the table are mainly referring to the amount of each metal ion that can be consumed each day, but the relative amounts allowed for each ion gives an idea of its toxicity in relation to the other ions. For instance, 5 times more zinc can be taken into the body each day than copper, suggesting that copper is more toxic to the body than zinc.

Table 1. A table from a University of Cagliari study showing healthy amounts of various metal ions.[16]

Element	Amount in 70 kg Human	Daily allowance
Mg	22 g	0.3 g
Mn	12 mg	3 mg
Fe	4 g	10-20 mg
Co	1 mg	3 μg (vit. B12)
Cu	80 mg	3 mg
Zn	2.3 g	15 mg

Previous studies have already shown that nontoxic antimicrobial zinc-based MOFs can be synthesized.[15] One such study investigated the biocompatibility and antimicrobial properties of a

zinc(II)-carboxylate coordination polymer (Zn-CPP).[17] This paper found that the Zn-CPP could demonstrate high antimicrobial activity against *B subtilis, S. aureus, S. enteriditis, E. coli, P. vulgaris, and P. aeruginosa* while maintaining low host toxicity. The researchers in the study predicted that the antimicrobial activity functioned through chelation. The researchers also mentioned that the nanorod crystal structure used may have played a role in preventing bacteria from adhering to surfaces. Interestingly, the study also showed that alteration of the Zn-CPP shape could be achieved through minute changes to reaction conditions.[17] The biocompatibility of the metal ion used is of high importance, but it would also be ideal for the organic ligands to be biocompatible as well. One study has already shown that chelidonic acid (the ligand used in our study) in doses less than 20 mg/kg in mice does not result in any obvious signs of toxicity.[18] However, even though H_2CDO is biogenic, this same study also showed that it may be involved in suppression of immune system components such as immunoglobulin E (IgE), mast cells, and B/T lymphocytes.[18] Future studies may further investigate the biocompatibility of chelidonic acid.

B.2 Project Objective

This project aimed to consistently generate a zinc-based MOF $[(Zn(C_7H_2O)(H_2O)(C_5H_5N)_2)]_n$ with a similar structure to the copper-based me137 $[(Cu(C_7H_2O)(H_2O)(C_5H_5N)_2)]_n$. Me137 is already known to possess antimicrobial properties, so the zinc analogue was synthesized to offer a more biocompatible alternative. Another purpose of this study was to determine reproducible reaction conditions for the synthesis of Zn-based MOFs of varying molecular structures and physical morphologies. As mentioned previously, the physical appearance of the MOF does not necessarily correlate with the structure of the

framework; thus, it is essential that specific conditions are determined to achieve MOFs of particular structures. Powder X-ray diffraction (PXRD) analysis is essential for phase identification, comparing the structures of the synthesized MOFs to calculated data from SCXRD. Any alternate peaks on the PXRD diffractograms could indicate differences in framework structure. On the other hand, the PXRD should show relatively identical peaks for two samples, providing strong support that two samples are structurally identical.

In general, for the Compound 1, a large, individual (e.g., no clusters or twinned xtals) crystal is ideal for single crystal analysis (to determine the structure), while a small particle size (e.g., nanoparticles, high surface area) is likely preferred for actual biomedical applications (see Figure 2).

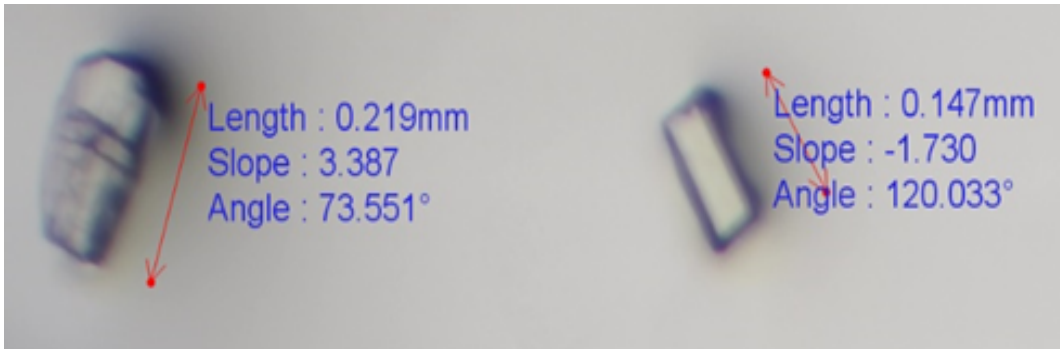

Figure 2. Left- An image of more amorphous crystals. Right- An image of a high-quality single crystal that would be ideal for SCXRD analysis. The single crystal is a similar size to the degraded crystal.

After consistent and specific synthesis conditions were obtained, this study transitioned to investigating the antimicrobial properties of the target biocompatible MOFs. In particular, Compound 1 was tested against *Staphylococcus aureus* and *Escherichia coli*, two of the most common bacteria associated with postoperative hernia infections.[2] Further research explored the ability of the MOFs to adhere to various surfaces. Hernia meshes are primarily composed of

polypropylene (PP), polytetrafluorethylene (PTFE), ePTFE, or polyester, so adhesion tests focused on polypropylene.[2]

C. Results

C.1 Materials and Methods

All chemicals were used as purchased. Powder X-ray diffraction data was collected via a Bruker D_2 Phaser CCD diffractometer. Single-crystal X-ray diffraction (SCXRD) data was obtained from a previous paper and on a Bruker AXS Diffractometer at Florida Gulf Coast University.[11] Additional SCXRD data was acquired from Dr. Lukasz Wojtas at the University of South Florida. Thermogravimetric analysis data was collected via a TA Instruments TGA Q50. Absorbance studies were obtained via a Gen5 BioTek Spectrometer. Fresh dimethylformamide (DMF) was used to limit the amount of water present. Chelidonic acid monohydrate was used for all samples in this research. The structures of the chemicals used in this experiment are depicted in Figure 3.

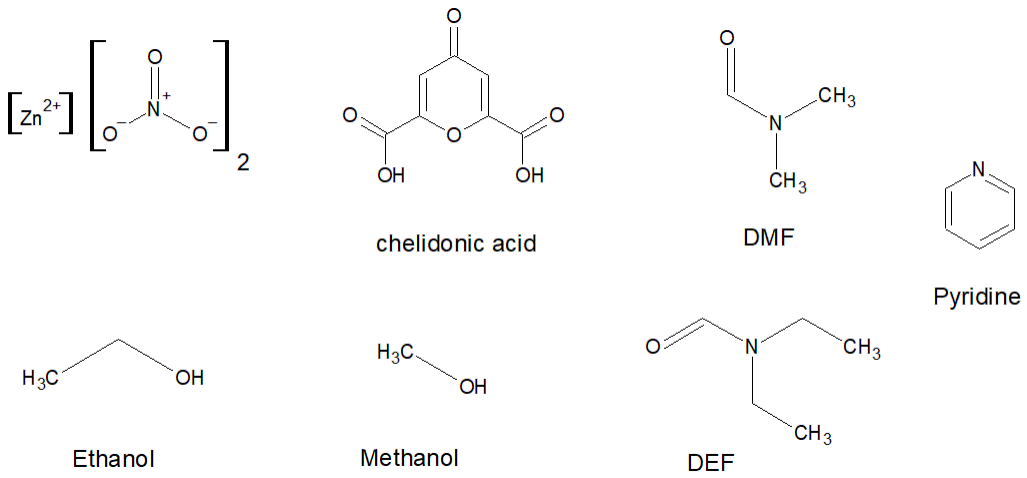

Figure 3. Reagents used for Compound 1 and 2**.** Either methanol or ethanol could produce compound 1, but the addition of UV light caused conversion of Compound 1 to Compound 2.

C.1.1 Reaction Conditions and Resulting Zn-based MOFs

One recent study has investigated metal-organic frameworks produced with zinc as the metal and chelodinate as a ligand.[10] However, that study did not utilize the same solvent systems utilized in this project. Information about the unit cells for me137 and Compound 1 are shown in Table 6. Data depicting the reaction conditions and resulting crystal morphologies is shown in the tables and figures below.

Table 2. Conditions and Observations for Compound 1, Method 1 (RV19.7-19.9)

Vial	M/L	M (in DMF)	L (in DMF)	DMF	MeOH	py	Observations
RV19.7	1.0 ml	0.5 ml	0.5 ml	0 ml	1.0	0.1 ml	Small, powdery gray crystals. Cube-shaped but low quality. Multiple instances of nucleated growth
RV19.8	1.0 ml	0.5 ml	0.5 ml	0 ml	1.5 ml	0.1 ml	Small, powdery gray crystals. Cube-shaped with no visible single crystals. Jagged surface.
RV19.9	1.0 ml	0.5 ml	0.5 ml	0 ml	2.0 ml	0.1 ml	Moderately-sized gray crystals. Cube shaped with some visible single crystals. Mixture of crystals with jagged and smooth surfaces.

Table 3. Conditions and Observations for Compound 1, Method 2 (RV9.14-9.16)

Vial	M/L	M (in DMF)	L (in DMF)	DMF	EtOH	py	Observations
RV9.14	1.0 ml	0.5 ml	0.5 ml	0 ml	1.0 ml	0.1 ml	Small rectangular prism shape. Clumping.
RV9.15	1.0 ml	0.5 ml	0.5 ml	0 ml	1.0 ml	0.1 ml	Needle-like crystals. Small individual crystal size. Yellowing of solvent (could indicate it was heated for too long)
RV9.16	1.0 ml	0.5 ml	0.5 ml	0 ml	1.0 ml	0.1 ml	Clustered/nucleated. Crystals more needle-like/rectangular in shape. Small individual crystal size.

Table 4. Conditions and Observations for Compound 1, Method 3 (RV23-25)

Vial	M/L	M (in	L (in	DEF	EtOH	py	Observations

		DEF)	DEF)				
RV23	1.0 ml	0.5 ml	0.5 ml	1.0 ml	0	0.1 ml	Crystals more clustered. Some more rectangular in shape and some more round/powdery
RV24	1.0 ml	0.5 ml	0.5 ml	0.5 ml	0.5 ml	0.1 ml	Very powdery. Crystals much smaller than other reactions run. Clustering present
RV25	1.0 ml	0.5 ml	0.5 ml	0 ml	1.0 ml	0.1 ml	Small crystals. Most appear to be nucleated. Some rectangular in shape. Others needle-like

Table 5. Conditions and Observations for Compound 1, Method 4 (RV30.1-30.3)

Vial	M/L	M (in DEF)	L (in DEF)	DEF	MeOH	py	Observations
RV30.1	1.0 ml	0.5 ml	0.5 ml	0 ml	2.5 ml	0.1 ml	Noticed clumping of the reagents in the bottom of the vial after adding all reactants. May need to increase sonication in future for better mixing. Possible explanation for why first vial seems to have clumped crystals after heating?
RV30.2	1.0 ml	0.5 ml	0.5 ml	0 ml	2.5 ml	0.1 ml	More cubic crystals, heavily clustered, relatively transparent crystals
RV30.3	1.0 ml	0.5 ml	0.5 ml	0 ml	2.5 ml	0.1 ml	More rectangular/needle-like crystals

C.1.2 Antimicrobial Assays

A modified version of the well-diffusion method was used to assess the antimicrobial properties of the Zn-based MOFs. This method involved first plating the desired bacteria on the Mueller-Hinton agar. Small holes (wells) were then made in the agar using a glass rod. Approximately equal amounts (in grams) of the materials to be examined were placed within these wells and the plate was placed in the incubator at 37℃ for 24, 48, or 72 hours. Presence of antimicrobial properties was determined based on the presence or absence of a zone of inhibition. The relative sizes of the zones were also noted. Some plates included holes with no test substance added to act as a negative control.

The antimicrobial properties of Compound 1 (and its ligands) were also assessed using spectrophotometry. 96-well plates were used to test varying combinations of bacteria (*E. coli* or *S. aureus*), substance (MOF or ligands), and media. Control wells were set up using only media (LB Broth) and only bacteria. Other wells were filled in with bacteria and the test substance. The plate was heated at 37 ℃ for 6-72 hours to allow for growth of the bacteria. During this 6-72 hour period, the spectrophotometer took readings of the absorbance values for each plate.

C.1.3 Polypropylene Adhesion

Vials were set up to produce Compound 1 crystals as described previously (see C.1.1). Polypropylene pellets were added to the vials prior to heating. The vials were then heated for 24 hours at 50℃. Growth of the MOF on the pellets was visualized using a light microscope and identity of the product was determined using IR and PXRD analysis.

C.2 Discussion

C.2.1 Synthesis of Compound 1 $[(Zn(C_7H_2O)(H_2O)(C_5H_5N)_2)]_n$

Thus far, two different Zn-based MOF structures have been identified. Figure 3 depicts the reagents used for the two Zn-based MOF structures. The difference between the two is that methanol was used for Compound 1 while ethanol was used for RV9.16 (also Compound 1). However, RV9.16 (originally Compound 1) was then exposed to light, causing conversion to Compound 2.

Figure 1 shows the predicted structure of Compound 1. Hydrogen bonding occurs between water molecules of one chain and chelidonates of another, which further increases stability (Figure 1). The unit cell of Compound 1 consists of two overlapping chains where the pyridine and chelidonic acid ligands are in close proximity to each other. It is thought that the proximity of the pyridines contributes to the overall stability of the MOF through π-π stacking

interactions. For each zinc ion, there are two chelidonate bridging ligands, two pyridine terminal ligands, and one water terminal ligand, and the coordination geometry around the zinc is trigonal bipyramidal (Figure 1). The Zn-MOF chain consists of alternating zincs and chelidonates.

Single crystal analysis has been done on RV19.9 and RV22 (both Compound 1). The results of the analysis were obtained for RV22. These results showed that Compound 1 had a nearly identical structure compared to me137. One key difference between RV22 and me137 that was noted was that the overlapping pyridines were in closer proximity in RV22 than in me137 (Table 6). This could suggest that RV22 is more stable due to stronger π-π stacking interactions, but further testing and analysis will be required to confirm this.

Table 6. Unit Cell Data for RV22 and me137.

MOF	a	b	c	α	β	γ
RV22	8.8355	10.0819	10.6203	63.116	84.028	77.969
me137	8.738	10.188	10.760	63.080	83.713	76.770

C.2.1.1 Control of Crystal Morphology

Changes to the solvent systems were made with the intent to alter crystal morphology without changing inherent lattice structure. Tables 2-5 show the conditions used to synthesize the zinc-based MOFs. Varying combinations of ethanol, methanol, N,N-dimethylformamide (DMF), and N,N-diethylformamide (DEF) were used to generate different solvent systems. As seen in the images in Tables 2-5, the changing quantities/types of solvents used altered the morphologies (shapes) of the crystals drastically. In Figure 4, the solvent system consisting of methanol and DMF (Method 1) is shown to produce crystals that are more cube-like. Ethanol and DMF

(Method 2) produces crystals that are more like rectangular prisms or needles (Figure 5). A mixture of DEF and ethanol (Method 3) produces small microcrystals (Figure 6). Previous trials had been run at 85℃ in an oven, but the Zn-based MOF tended to quickly degrade at this temperature. As a note, degradation in this case is being defined as an increase in cloudiness and cracking (see Figure 2 (Left)) for an example of a "degraded" crystal). To reduce degradation, allow for higher quality crystal growth, and reduce unnecessary power usage for the reaction, the temperature was reduced to 50-55℃ and the vials were placed in a sand bath on a hot plate instead of in an oven. The logic behind this change was that a lower temperature would allow for the crystals to grow at a slower, more controlled pace. All samples shown in Tables 2-5 were heated in the sand bath on the hot plate. Overall, the observations from Figures 4-6 suggest that three crystal morphologies (cube, rectangular prism, microcrystal) can be produced in the zinc/CDO-based MOFs.

The Zn-based structure from this study Compound 1 ($[(Zn(C_7H_2O)(H_2O)(C_5H_5N)_2)]_n$) has a similar structure to me137. Figures 4, 5, and 6 show that the peaks for the Zn-based MOFs using different solvent systems (Methods 1-3) are nearly identical to the peaks for me137 and Compound 1.

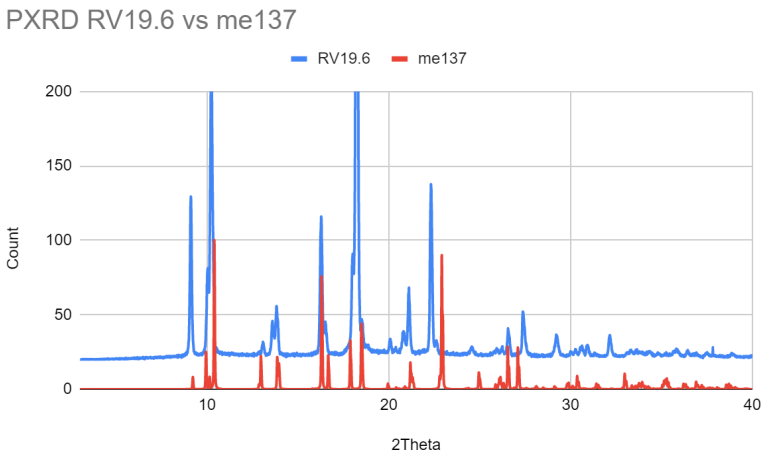

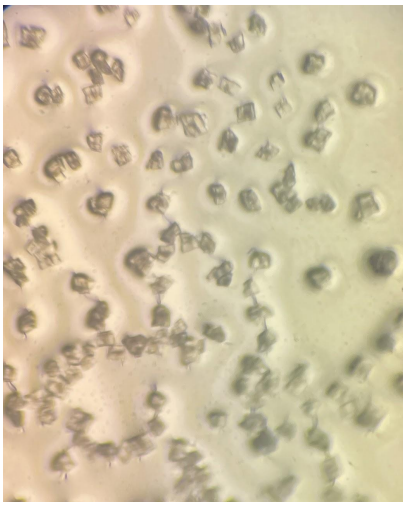

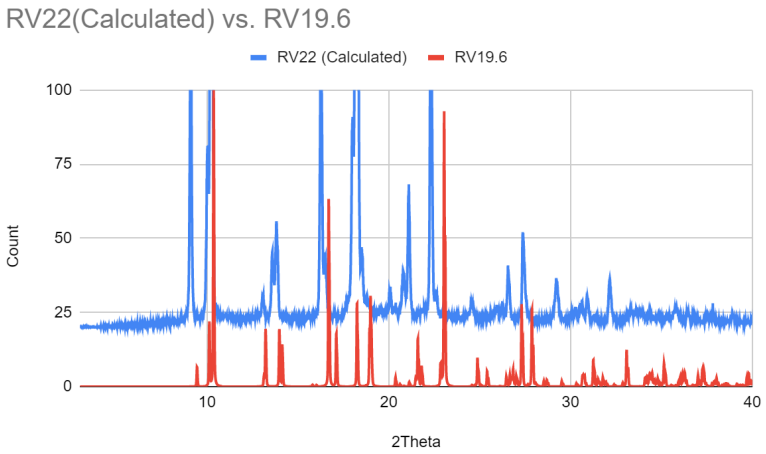

Figure 4. Left - Diffractogram of RV19.6 and me137. RV19.6 was synthesized with a 1 DMF: 2 MeOH solvent system**.** Right - Image of RV19.6. Bottom - PXRD of Compound 1 vs. RV19.6 (See Table 2).)

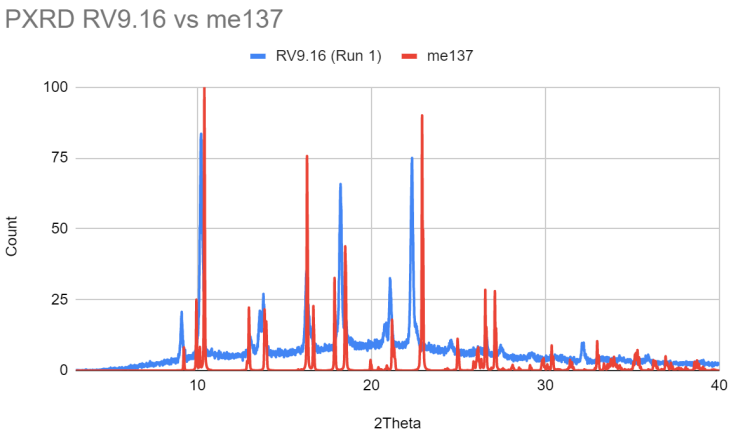

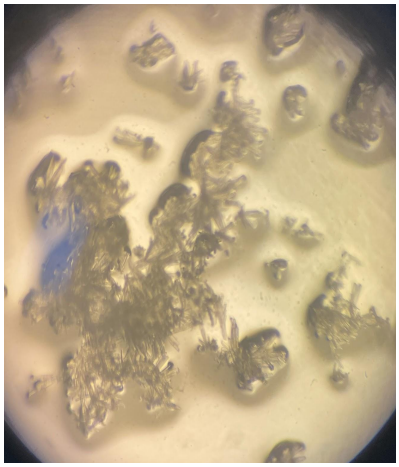

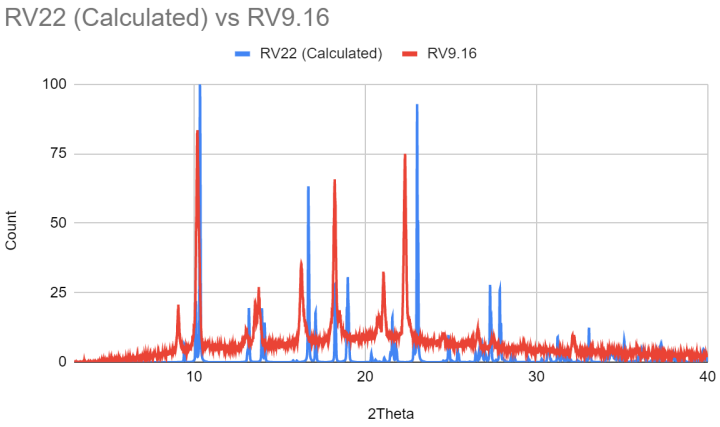

Figure 5. Left - Diffractogram of RV9.16 (not photo product) and me137. RV9.16 was synthesized with a 1 DMF: 1 EtOH solvent system. Right - Image of RV9.16. Bottom- PXRD of Compound 1 vs RV9.16 (see Table 3).

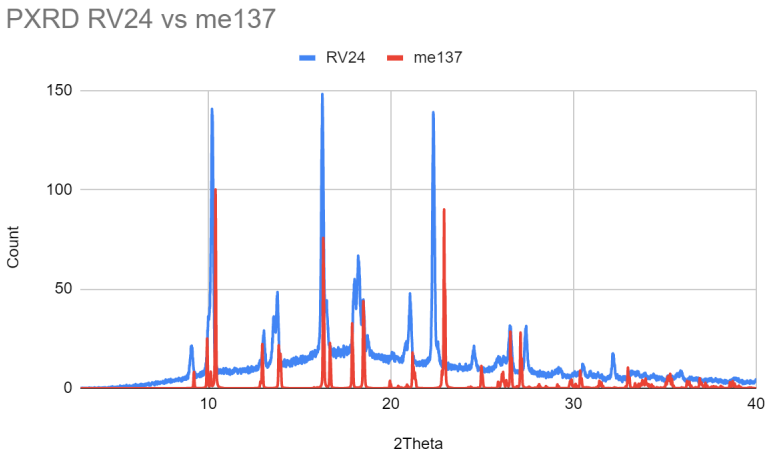

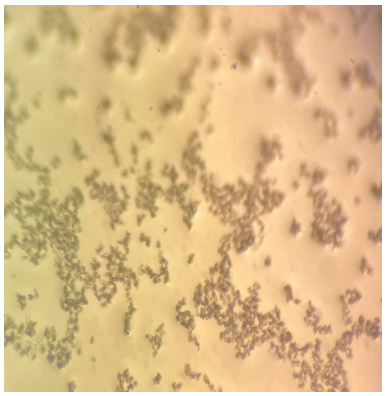

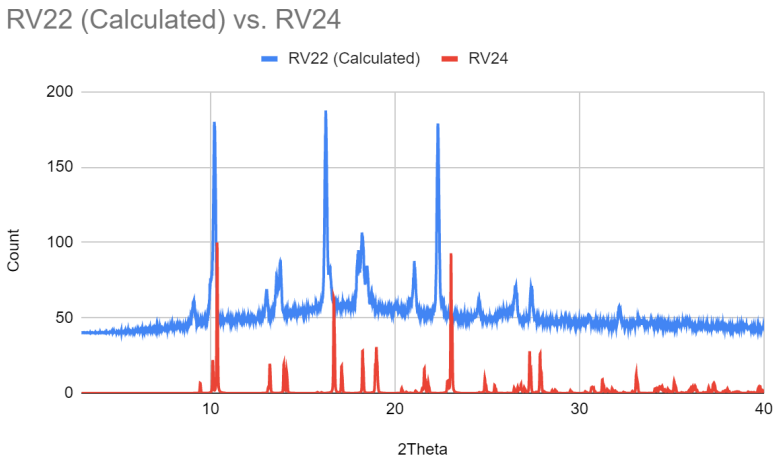

Figure 6. Left - PXRD of RV24 and me137. Crystals were synthesized with a 3 DEF: 1 EtOH solvent system. Right - Image of RV24. Bottom- PXRD of Compound 1 vs RV24 (See Table 4).

However, all Zn-based MOFs demonstrate one particular peak that is distinctly different from the me137 PXRD. In the Zn-based MOFs, there is a large peak at around 22°. This peak is shifted in me137. Me137 possesses a peak at 24, but the fact that all Zn-based MOFs showed the peak at almost precisely 22.3° every time suggests that the peak is not the result of random error. The small difference in the PXRD results means that the Zn-based MOFs are similar in structure but could mean they are not entirely identical. An identical comparison can be made between RV24 and the calculated PXRD for Compound 1. Most of the peaks align well, but there is a difference at the 22.3° peak. It is possible that the zinc has a different molecular geometry compared to copper, causing slight deviation in the angles of the structure. The possible molecular geometries for zinc are depicted below in Figure 7. However, another explanation for this discrepancy could be differences in the parameters used to calculate the ideal values for me137/Compound 1 (RV22) and the parameters used to measure the peaks for the experimental data. More specifically, the step for the software calculation may have been different than the

actual step used during measurement. This hypothesis could explain why even the calculated PXRD for Compound 1 differs from the measured values for samples that should also be Compound 1.

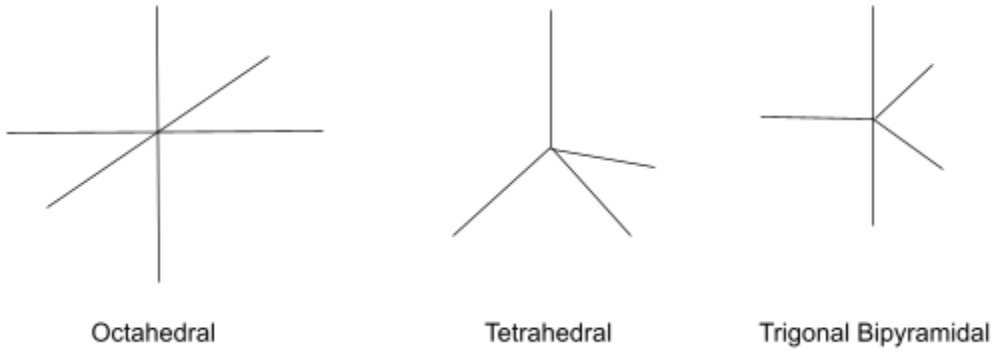

Figure 7. Coordination geometries for zinc. Zn-MOFs are expected to exhibit trigonal bipyramidal geometry.

Figures 4-6 showed that the morphologies of the MOFs changed, but the PXRD patterns demonstrated that the crystal structures did not. As seen in Figure 8, all of the Zn-based MOFs produce nearly identical PXRD peaks.This indicates that the chemical structures of the MOFs are the same or nearly the same. The differences in peak intensities can likely be attributed to preferred orientation. In other words, since the crystals demonstrate different morphologies, they may be more likely to be oriented differently in 3D space. Small differences in crystal orientation can cause some X-ray diffraction angles to be disproportionately represented in the PXRD graph.

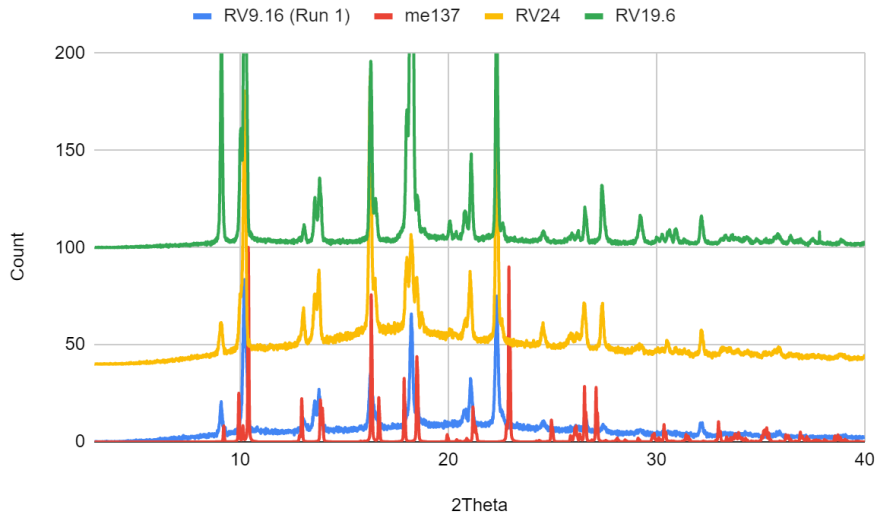

Figure 8. Diffractogram of RV19.6, RV9.16 (not photoproduct), RV24, and me137.

C.2.1.2 Photodimerization of Compound 1 to Form Compound 2

A previous study has demonstrated that proximal chelidonate ligands can dimerize in the presence of light to form a tetraasterane-like ring.[11] The presence of a photoproduct, Compound 2, is supported by the PXRD shown in Figure 9.

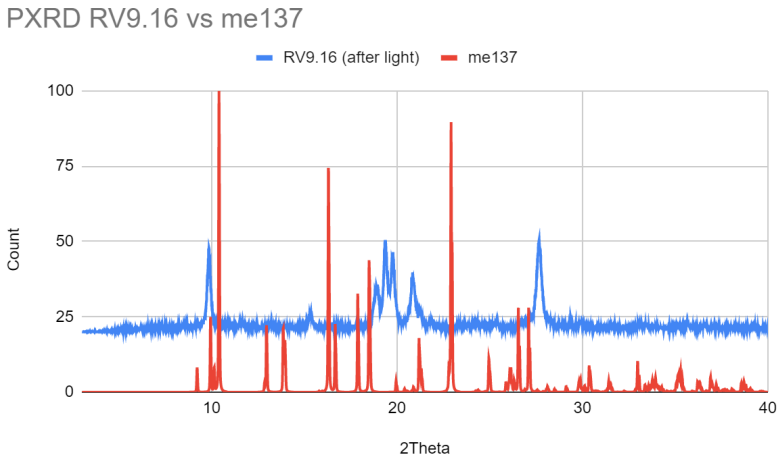

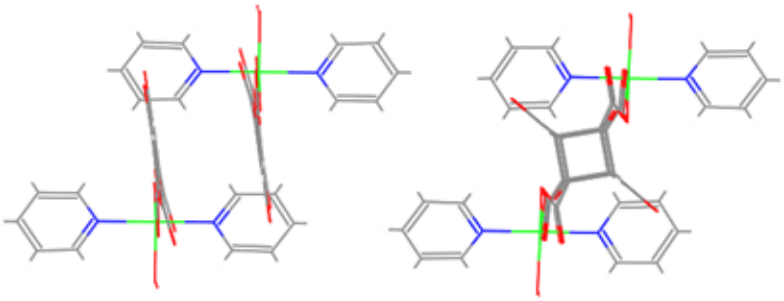

Figure 9. Top - Diffractogram of RV9.16 (photo product) and me137. Bottom - Image of me137 structure (left) vs me201 (photodimer) structure (right).[11]

Prior to light exposure (Figure 5), RV9.16 possessed a similar PXRD to me137. However, after exposure to light, the PXRD drastically changed. Nearly every peak for Compound 2 in Figure 9 is different from the original structure peaks and is therefore different from the me137 peaks as well. This rapid change in structure suggests that a photoproduct was formed. In addition, no other samples of Compound 1 converted to Compound 2. This could be due to the fact that Compound 1 samples were stored in a dark cabinet. Although some new MOF, Compound 2, appears to have formed, there is not yet enough evidence to suggest that the photoproduct formed is the same as the one from the study by Eubank et al.[11] A comparison of the PXRD for me201, the photoproduct from the aforementioned study, does not match well with the PXRD of RV9.16 (Figure 10).

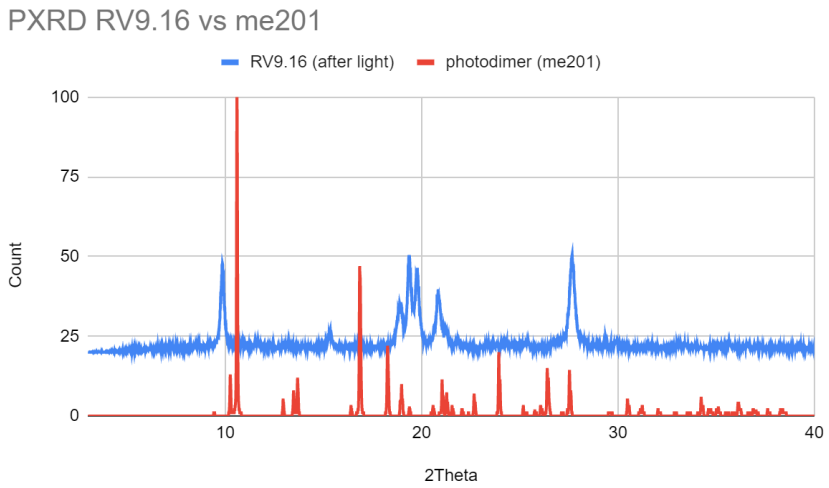

Figure 10. PXRD of Compound 2 (photoproduct) and me201.[11]

C.2.2 Thermogravimetric Analysis of Compound 1

TGA was performed for Compound 1 to determine further information about the composition of the MOF. The important temperatures associated with mass loss in the TGA data were at 119 ℃, 161℃, and 268℃. The drop in mass beginning at 119℃ likely corresponds to the loss of water. This prediction is supported by the 5.24% drop in mass after 119℃ (Figure 11). Based on the predicted molecular formula for Compound 1, water should constitute approximately 5.49% of the total molecular weight. The drop in mass at 161℃ may correlate with the evaporation of excess diethylformamide. The mass loss at 268℃ may be due to the loss of the chelidonate bridging ligands. Chelidonate constitutes 29.7% of the total MW of Compound 1, and the mass loss after 268℃ was approximately 33.37% (Figure 11). Comparison of these values results in a percent difference of only 11.63%, which supports the hypothesis that the loss of chelidonate is the major reason for the mass loss at 268°C.

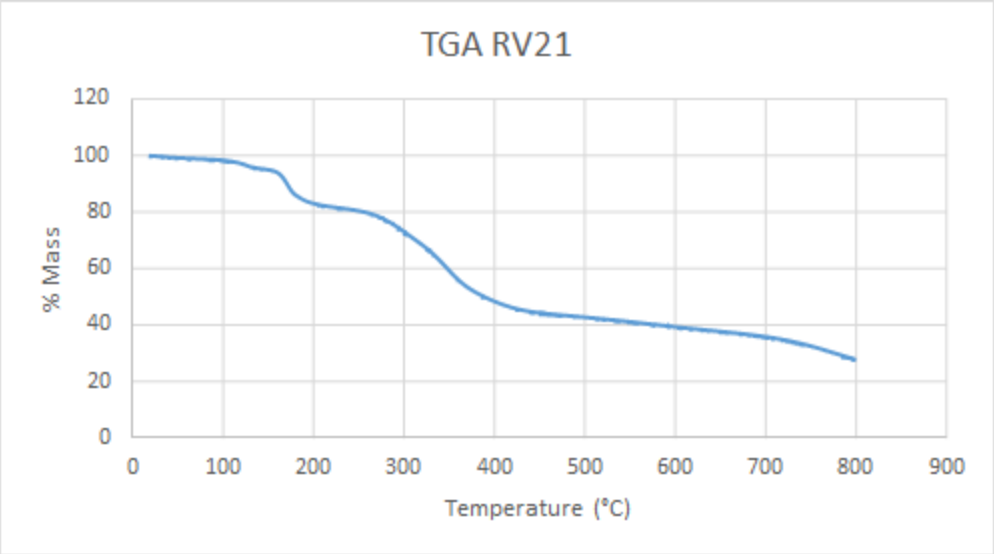

Figure 11. TGA data for RV21. Key points of mass loss occur at 119 ℃, 161℃, and 268℃.

Overall, Zn-based MOFs appear to be more resistant to structural change under varying conditions. Cu-based MOFs were synthesized with the same solvent system as RV9.14-16 for comparison. With the Cu-based MOFs, it was noted that even changes in humidity could alter the chemical structure, resulting in conversion of one MOF structure to another. Compound 1, however, does not seem to be affected by humidity or different solvent systems to the same degree that the Cu-based MOFs are. As demonstrated by the PXRD data, even when vastly different solvent systems (methanol and DEF, ethanol and DMF, etc.) were used, the resulting structure was the same. Another trend in the data is that more dilute solutions (more methanol) tended to produce higher quality crystals (for an example of a "high quality crystal" see Figure 2). It is possible that this trend was, in part, due to the solubility of zinc nitrate and chelidonic acid in the chosen solvent systems. When compared to the synthesis of analogous Cu-based MOFs, the Compound 1 components appeared to demonstrate lower solubility in the mother

solutions. For instance, rather than requiring 1-2 minutes of sonication to achieve a homogenized solution, Compound 1 required upwards of 5-6 minutes.

C.2.3 Antimicrobial Assays

Antimicrobial assays were performed on Compound 1 to determine both the potency of its antimicrobial properties and the mechanism behind these properties. Initial experiments assessed potency through the use of the well-diffusion method of bacterial testing (see materials and methods).[19] The clear zone of inhibition produced by the Compound 1 (Figure 12 (Middle/Right)) demonstrated that Compound 1 did indeed possess antimicrobial properties.

After it was determined Compound 1 had antimicrobial properties, further experiments were performed to compare the potency of Compound 1 to the potencies of its constituents. Based on the relative sizes of the zones of inhibition, Compound 1 initially appeared to be less potent than zinc nitrate hexahydrate but more potent than chelidonic acid (Figure 12 (Middle)). However, additional experiments revealed that the discrepancy between Compound 1 and zinc nitrate may, in part, be due to a difference in the ability to diffuse throughout the agar. Compound 1 remains in crystalline form even after incubation, meaning that it is not able to spread as far through the agar. The smaller size of the Compound 1 zone of inhibition could, therefore, be due more to physical limitations than the antimicrobial potency. This prediction was supported through experiments performed on zinc nitrate by itself (Figure 12B). Even in the absence of *E. coli*, a large white zone is produced by the zinc nitrate. Since this zone is opaque, it is difficult to determine the true size of the zone of inhibition. Future investigations may examine the distance the RV22 MOF is able to diffuse through the agar.

The mechanism of Compound 1's bacterial action was also briefly investigated. This was done by attempting to transfer a swab of bacteria from the zone of inhibition of one plate to another plate. If the mechanism were bactericidal, one would expect no bacteria to grow on this new plate since all of the bacteria within the zone of inhibition would be dead. However, the plate resulted in bacterial growth, suggesting that the mechanism may be bacteriostatic (Figure 12 (Left)). Further trials need to be performed to make any conclusions. Other research has more accurately determined antimicrobial mechanisms through the use of Raman spectroscopy, so future experiments may incorporate this form of analysis.[20]

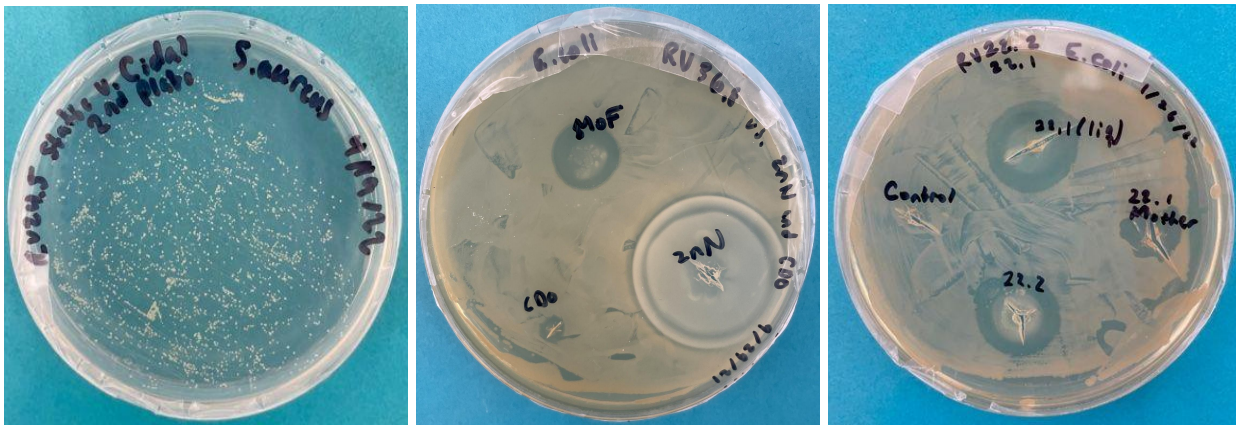

Figure 12. Left - Image of plate *S. aureus* that was cultured from the zone of inhibition from another plate (not shown). Middle - Image of plate containing *E. coli* and RV36.8. There are wells for the MOF, zinc nitrate (ZnN), and chelidonic acid (CDO). Right - Image of plate containing *E. coli*, RV22.2, and RV22.1.

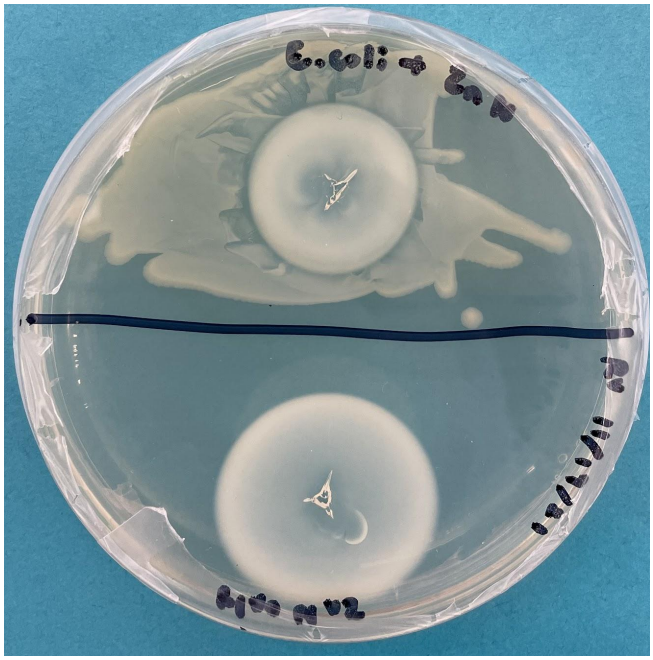

Figure 12B. Image of plate containing *E. coli* and zinc nitrate in the upper half and only zinc nitrate in the lower half.

Other experiments that were performed assessed the antimicrobial properties of Compound 1 in its mother solution (Figure 12 (Right)). The mother solution produced a zone of inhibition, meaning that future experiments had to be done using dried Compound 1 to mitigate the impact of the solvents.

C.2.3.1 Absorbance Experiments

Experiments to further characterize the antimicrobial properties of Compound 1 were performed. The absorbance studies aimed to analyze the antimicrobial potency of Compound 1 against *E. coli* and *S. aureus* in a liquid broth rather than in solid agar. The results from these absorbance tests did not suggest any significant antimicrobial activity by Compound 1 (Figure 13). Had Compound 1 exhibited the ability to inhibit bacterial growth in a liquid culture, the growth rates of the bacteria during their "log phase" would have been diminished or stopped.

The changes in absorbance over time did not follow predictable patterns for the experiments involving *S. aureus*. However, the experiments with *E. coli* did produce quantifiable patterns. The average rate of change in absorbance for C1-C4 was 0.315. The average rate of change in absorbance for B1-B3 was 0.0910. These results are the opposite of what is expected. Based on this limited data, it appears that the addition of Compound 1 may have even increased bacterial growth rate. However, this conclusion cannot simply be made. Not only is the sample size to confirm anything, but also there are several inconsistent results. For instance, in well C1, the absorbance increased rapidly and then began to decrease slowly over time. After 48 hours, the absorbance spiked again. This result does not conform with the rest of the data and suggests there were potentially other variables influencing the results. The inconclusive results from this experiment are not necessarily indicative of a lack of antimicrobial potency by Compound 1, however. The study by Wang, et. al mentioned that a possible mechanism of action for antimicrobial compounds is prevention of bacterial adhesion.[17] In that study, the researchers specifically noted that their nanorod structures may have been preventing adhesion of bacteria to their test surface due to clustering of "nanorod-flower" particles. It is possible that Compound 1 inhibits bacterial growth through a similar mechanism. Since the absorbance tests were done exclusively in liquid broth, there was no surface to which bacteria could adhere in the first place, thus potentially stymying Compound 1's antimicrobial efficacy.

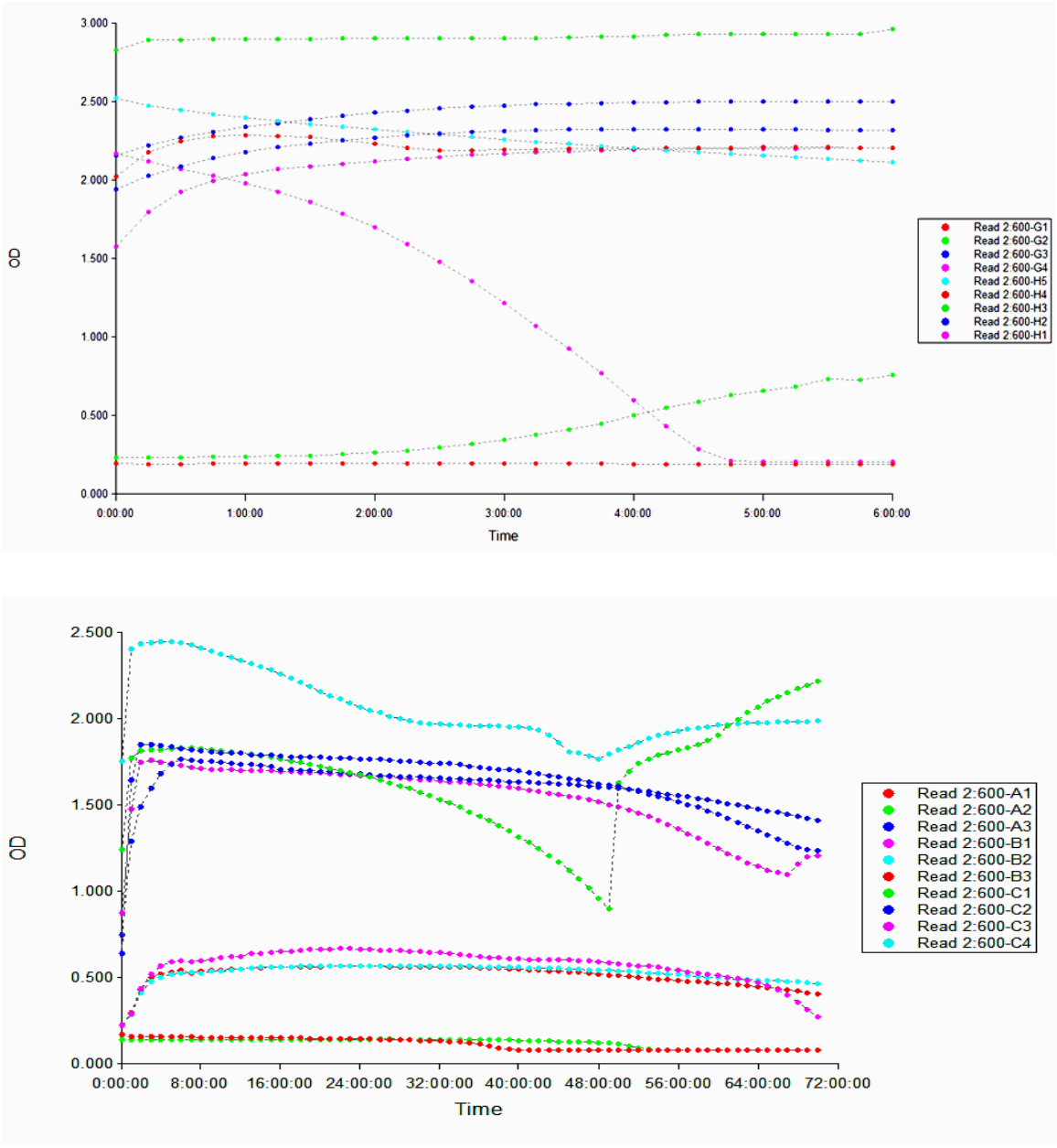

Figure 13. Top - G1=TB broth, G2=*S. aureus*, G3=TB broth + Comp. 1, G4=TB broth + chelidonic acid (CDO), H1=*S. aureus*+Comp. 1 in mother soln., H2=*S. aureus*+Comp. 1 in mother soln, H3=*S.aureus*+Comp. 1 dry, H4=*S. aureus*+Comp. 1 dry, H5=*S. aureus*+CDO. Bottom- A1=TB broth, A2=TB broth, A3=TB broth+Comp. 1, B1=*E. coli*, B2=*E. coli*, B3=*E. coli*, C1=*E. coli*+Comp. 1 dry, C2=*E. coli*+Comp. 1 in mother soln, C3=*E. coli*+Comp. 1 dry, C4=*E. coli*+Comp. 1 dry.

C.2.4 Growth of Compound 1 on Hernia Mesh

Since the Zn-MOFs have demonstrated antimicrobial properties, experiments were performed to attempt to grow the MOFs on hernia mesh materials. A previous study has shown that growth of ZIF-8, a MOF with imidazolate ligands, could be grown on polypropylene.[22] Polypropylene is one of the more common hernia mesh materials, so a similar method as the one used in the aforementioned study could be employed. The method used is known as fast current-driven synthesis, where a direct current is used to promote growth of the MOF on the polypropylene. Other synthesis methods have also been investigated. For instance, it may be possible to first convert polypropylene into poly(acrylic acid) via a reaction with an oxidizing agent. This poly(acrylic) acid may then be able to interact with the zinc metal through coordination via its carboxylic acid. This poly(acrylic acid) could replace either a terminal ligand (such as pyridine) or a bridging ligand (chelidonic acid) (Figure 14).

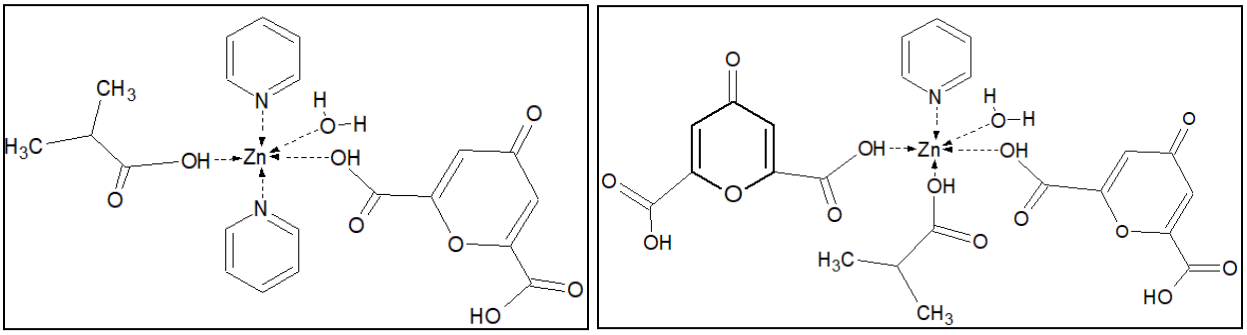

Figure 14. Left- Depiction of poly(acrylic acid) replacing chelidonic acid in RV19.9. Right - Depiction of poly(acrylic acid) replacing pyridine in RV19.9. Note that the poly(acrylic acid) in these images is only shown as one monomer rather than a polymer.

In this experiment, however, a more rudimentary approach was taken. Initial tests involved placement of the mesh materials (polypropylene and poly(acrylic acid)) into vials containing the reagents for Compound 1. The vials were then put through the same conditions as

those used in the synthesis of Compound 1 by itself. Initial observation of the resulting crystals under the microscope indicated that Compound 1 crystals were growing on the surface of the polypropylene pellets (Figure 15 (Left)).

Figure 15. Left- Microscope image of polypropylene pellet placed in RV22 conditions. Right- Image of poly(acrylic acid) placed in Compound 1 conditions.

To confirm the growth of Compound 1 on the polypropylene, PXRD analysis was necessary. Comparison of PXRD peaks before and after washing the polypropylene pellets demonstrated that there was not any apparent growth of the MOF on the surface of the polypropylene (Figure 16). There are few peaks that directly correlate between the two samples.

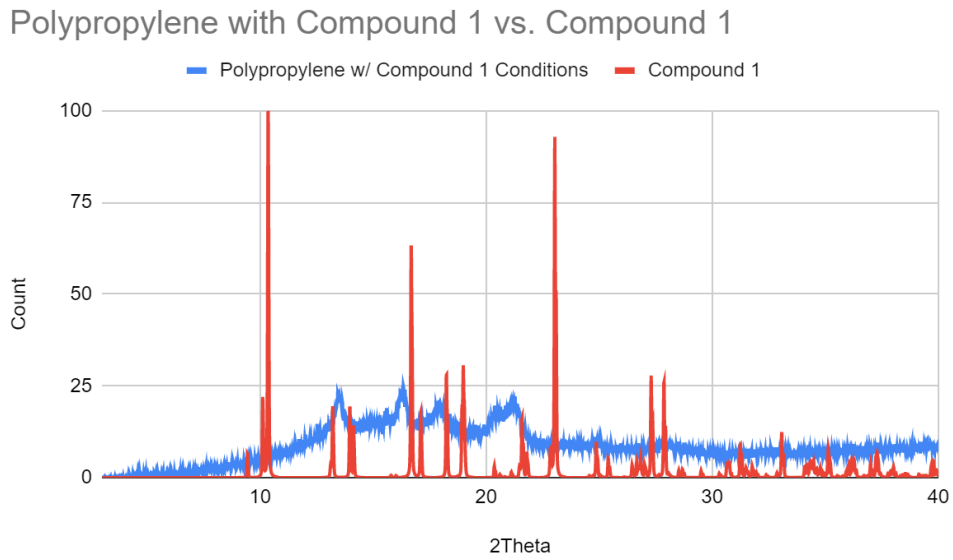

Figure 16. PXRD comparing polypropylene (Compound 1 conditions) (blue) to Compound 1 (red).

Experiments with poly(acrylic acid) netted unexpected results. Rather than producing a sheet of poly(acrylic acid) coated with Compound 1, the resulting mixture became a viscous gel that produced no crystals (Figure 15 (Right)). One possible explanation for this observation could be competition between the chelidonic acid and poly(acrylic acid) for binding to the zinc. Since chelidonic acid and poly(acrylic acid) both contain reactive carboxylic acid groups, they should both be able to interact with zinc ions; however, in this experiment, the poly(acrylic acid) is present in much higher quantities than the chelidonic acid. This imbalance in quantity could have caused the reaction to favor binding of zinc to poly(acrylic acid) rather than chelidonic acid, thus preventing the Compound 1 crystals from forming.

Due to the lack of success with growing Compound 1 onto unmodified polypropylene, further experimentation focused on methods of modifying functional groups of polypropylene to

allow for binding to zinc. The method that was explored was oxidation of polypropylene to poly(acrylic acid). The proposed scheme for this reaction is shown in Figure 17.

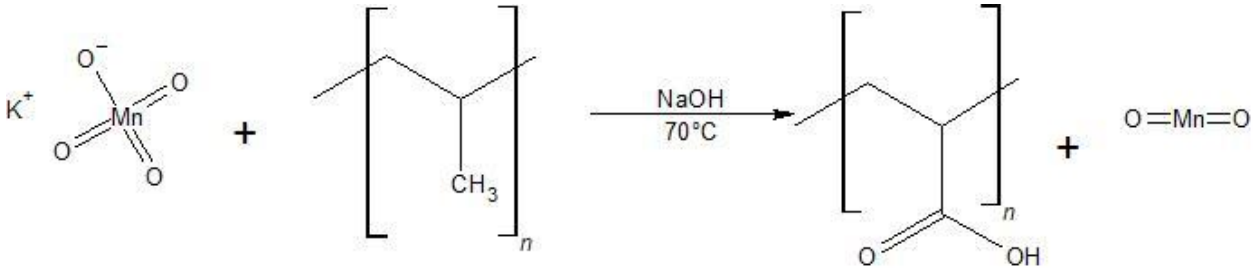

Figure 17. The proposed reaction scheme for the conversion of polypropylene to poly(acrylic acid).

C.2.4.1 Conversion of Polypropylene to Poly(acrylic acid)

Initial trials of the reaction to convert polypropylene to poly(acrylic acid) did not utilize NaOH. These trials did not appear to produce significant amounts of poly(acrylic acid) product, as evidenced by IR analysis (Figure 18). There does exist a weak peak at 3297.39 cm^{-1}, which could suggest conversion of small amounts of polypropylene to poly(acrylic acid), but the sample is clearly still largely composed of polypropylene.[23]

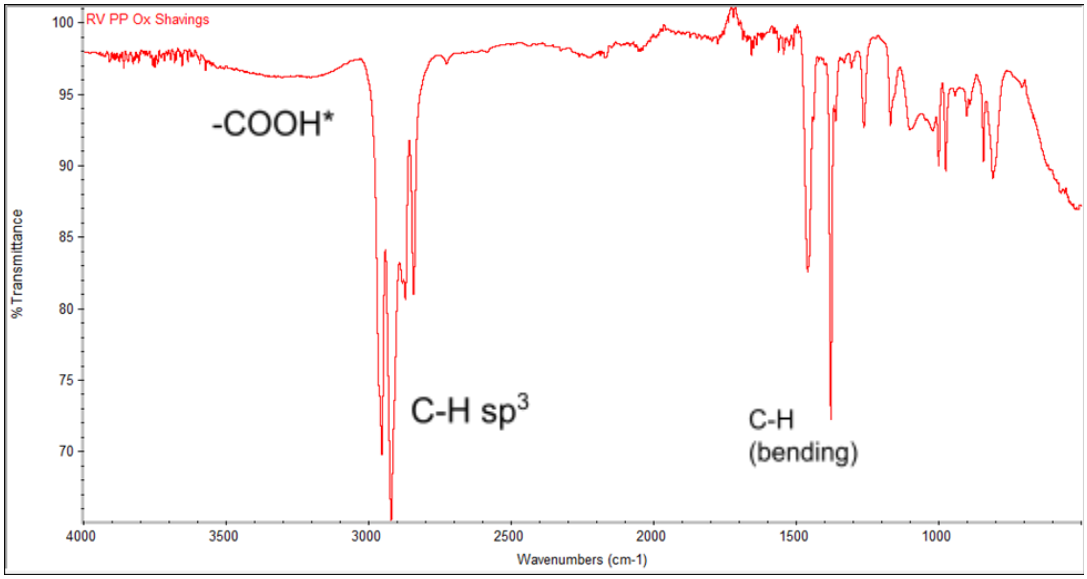

Figure 18. Infrared spectroscopy (IR) of polypropylene treated with $KMnO_4$ but not NaOH.

After running the reaction again for 7 days (without having added NaOH yet), NaOH was added and the reaction proceeded for 7 additional days in the hopes of pushing the reaction further toward the product. This method proved to be effective and resulted in the production of poly(acrylic acid). The conversion of polypropylene to poly(acrylic acid) was supported by IR analysis (Figure 19). Several key peaks from the IR strongly suggest that there was at least partial conversion of the polypropylene to poly(acrylic acid). For instance, the peak at 3335.41 cm^{-1} (Figure 19 (Top)) is consistent with a carboxyl functional group. This functional group is also present in poly(acrylic acid), as shown by the broad peak stretching from ~3500-3000 cm^{-1} (Figure 19 (Bottom)). In addition, the spectrum includes significant peaks at 1633.12 cm^{-1} and 913.44 cm^{-1} which are not present in untreated polypropylene. These peaks are predicted to correspond to a C=O bond and a C-O bond, respectively. Both of these bonds are present in poly(acrylic acid). One discrepancy between the spectra for the oxidized polypropylene and poly(acrylic acid) is the exact locations of these peaks. In poly(acrylic acid), the C=O peak is at 1696.61 cm^{-1} and the C-O peak is at 1163.65 cm^{-1} (Figure 19 (Bottom)). The discrepancy may be explained by a concept known as hydrogen bond blue-shifting.[24] This phenomena involves a decrease in wavenumbers due to hydrogen bonding. It is possible that the oxidized polypropylene is interacting with the MnO_2 by-product via hydrogen bonding, thus blue-shifting key peaks. This hypothesis is supported by the downward slope located in the fingerprint region of the oxidized polypropylene spectrum (Figure 19 (Top)). Previous studies have shown that downward slope in the fingerprint region of an IR graph can be indicative of MnO_2.[25]

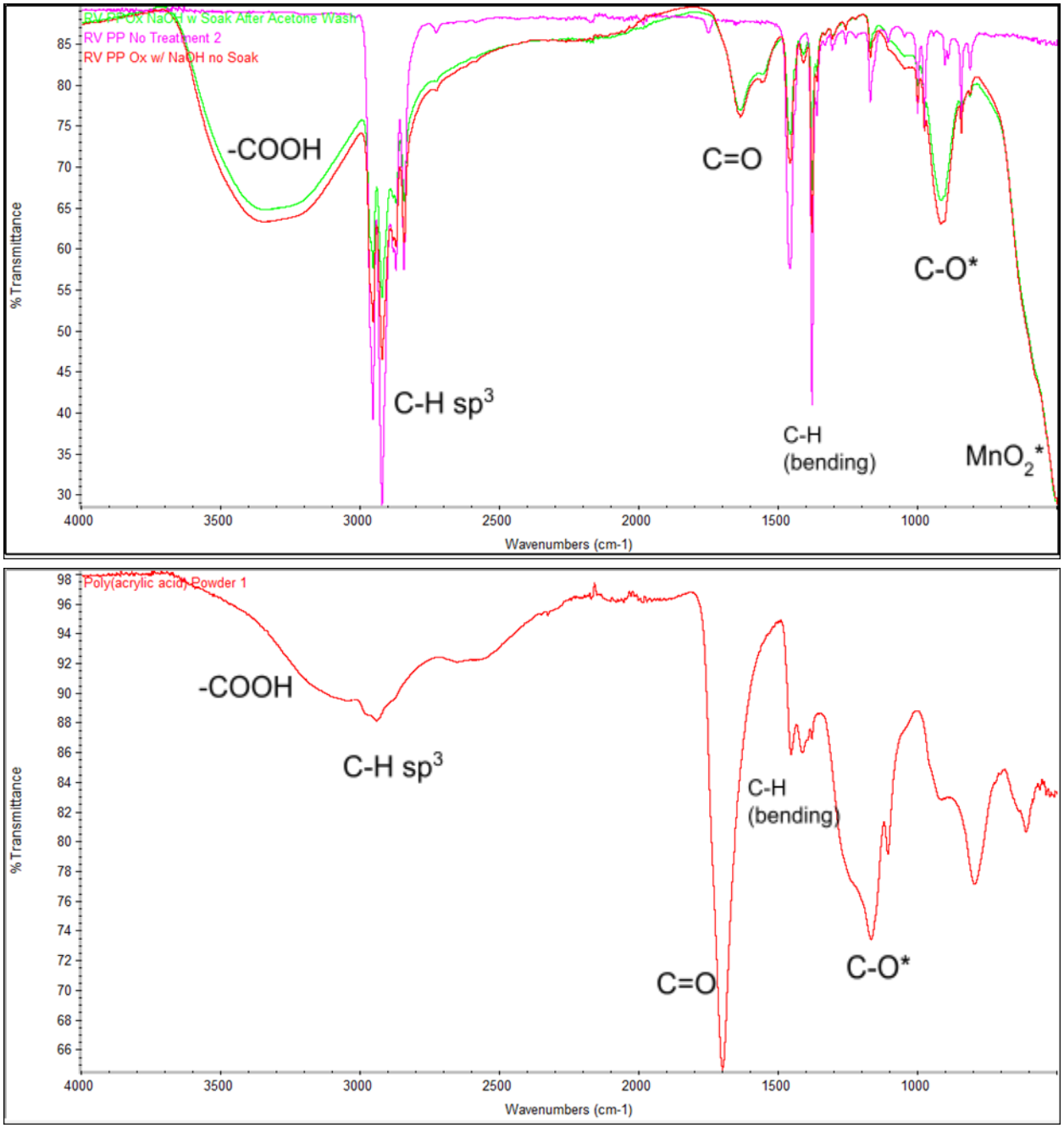

Figure 19. Top- IR of polypropylene (Purple) and polypropylene treated with the treatment described in Figure 16 (Red/Green). The red and green peaks refer to the same sample before and after an acetone wash, respectively. Bottom- IR of poly(acrylic acid) powder.

Note, the asterisks denote peaks where there is a degree of uncertainty regarding the interpretation.

D. Conclusion

Synthesis of a more biocompatible, Cu-analogous zinc-chelidonate MOF was successful. The new MOF, which is referred to as Compound 1, was synthesized using mild solvothermal synthesis. Its structure was determined through PXRD and single crystal analyses. Many different solvent systems and conditions were utilized, yet all resulted in the same substance, Compound 1. Factors that impacted similar copper-based MOFs such as humidity and temperature, appeared to have little impact on the synthesis/degradation of Compound 1. Thus, Compound 1 appears to be stable under a variety of conditions. After Compound 1 synthesis became reproducible, antimicrobial studies began to investigate its antibacterial potency. These studies have suggested that Compound 1 is capable of inhibiting the growth of *E. coli* and *S. aureus* through a bacteriostatic mechanism. Attempts to coat polypropylene in Compound 1 have been promising but have yet to yield successful products. There was success in converting polypropylene to poly(acrylic acid), but investigation of this newly synthesized poly(acrylic acid)'s ability to accommodate Compound 1 growth has not yet been tested.

Future experiments will further investigate the properties of Compound 2. The initial results from the exposure of RV9.16 to light are promising. They suggest that some form of photoproduct may have been produced; however, only one MOF has been exposed to light, so future tests will look into generating more photoproducts. Additionally, the PXRD of the RV9.16 photoproduct did not generate enough significant peaks to allow for conclusions to be made about its structure, so additional PXRDs will be acquired from any future photoproduct MOFs made. If Compound 2 can be made reliably, it will also be tested against bacteria for determination of the presence of antimicrobial properties. Other future experiments should focus on the stability of Compound 1 under different conditions. Its stability has already been shown in

varying levels of humidity and temperature, but new experiments need to be performed to determine its stability in conditions similar to the human body's. Experimentation will continue on the adhesion of Compound 1 to polypropylene and/or poly(acrylic acid). In addition, other hernia mesh materials (such as polyester) may be investigated as potential substitutes for polypropylene if polypropylene is deemed unsuitable.

References

(1)

Beadles, C. A.; Meagher, A. D.; Charles, A. G. Trends in Emergent Hernia Repair in the United States. *JAMA Surg* **2015**, *150* (3), 194. https://doi.org/10.1001/jamasurg.2014.1242.

(2)

Narkhede, R.; Shah, N. M.; Dalal, P. R.; Mangukia, C.; Dholaria, S. Postoperative Mesh Infection—Still a Concern in Laparoscopic Era. *Indian J Surg* **2015**, *77* (4), 322–326. https://doi.org/10.1007/s12262-015-1304-x.

(3)

Alezi, D.; Belmabkhout, Y.; Suyetin, M.; Bhatt, P. M.; Weseliński, Ł. J.; Solovyeva, V.; Adil, K.; Spanopoulos, I.; Trikalitis, P. N.; Emwas, A.-H.; Eddaoudi, M. MOF Crystal Chemistry Paving the Way to Gas Storage Needs: Aluminum-Based Soc-MOF for CH4, O2, and CO2 Storage. *J. Am. Chem. Soc.* **2015**, *137* (41), 13308–13318. https://doi.org/10.1021/jacs.5b07053.

(4)

Chaemchuen, S.; Zhou, K.; Kabir, N. A.; Chen, Y.; Ke, X.; Van Tendeloo, G.; Verpoort, F. Tuning Metal Sites of DABCO MOF for Gas Purification at Ambient Conditions. *Micropor Mesopor Mat* **2015**, *201*, 277–285. https://doi.org/10.1016/j.micromeso.2014.09.038.

(5)

Cui, Y.; Song, R.; Yu, J.; Liu, M.; Wang, Z.; Wu, C.; Yang, Y.; Wang, Z.; Chen, B.; Qian, G. Dual-Emitting MOF⊃Dye Composite for Ratiometric Temperature Sensing. *J Adv Mater* **2015**, *27* (8), 1420–1425. https://doi.org/10.1002/adma.201404700.

(6)

Llabrés i Xamena, F. X.; Abad, A.; Corma, A.; Garcia, H. MOFs as Catalysts: Activity, Reusability and Shape-Selectivity of a Pd-Containing MOF. *J Catal* **2007**, *250* (2), 294–298. https://doi.org/10.1016/j.jcat.2007.06.004.

(7)

Wang, C.; Qian, X.; An, X. In Situ Green Preparation and Antibacterial Activity of Copper-Based Metal–Organic Frameworks/Cellulose Fibers (HKUST-1/CF) Composite. *Cellulose* **2015**, *22* (6), 3789–3797. https://doi.org/10.1007/s10570-015-0754-4.

(8)

Aguado, S.; Quirós, J.; Canivet, J.; Farrusseng, D.; Boltes, K.; Rosal, R. Antimicrobial Activity of Cobalt Imidazolate Metal–Organic Frameworks. *Chemosphere* **2014**, *113*, 188–192. https://doi.org/10.1016/j.chemosphere.2014.05.029.

(9)

Akbarzadeh, F.; Motaghi, M.; Chauhan, N. P. S.; Sargazi, G. A Novel Synthesis of New Antibacterial Nanostructures Based on Zn-MOF Compound: Design, Characterization and a High Performance Application. *Heliyon* **2020**, *6* (1). https://doi.org/10.1016/j.heliyon.2020.e03231.

(10)

Carballo, R.; Lago, A. B.; Pino-Cuevas, A.; Gómez-Paz, O.; Fernández-Hermida, N.; Vázquez-López, E. M. Neutral and Cationic Chelidonate Coordination Polymers with N,N′-Bridging Ligands. *Chemistry* **2021**, *3* (1), 256–268. https://doi.org/10.3390/chemistry3010019.

(**11**)

Eubank, J. F.; Kravtsov, V. C.; Eddaoudi, M. Synthesis of Organic Photodimeric Cage Molecules Based on Cycloaddition via Metal-Ligand Directed Assembly. *J Am Chem Soc* **2007**, *129* (18), 5820–5821. https://doi.org/10.1021/ja070924n.

(12)

Chen, Q.; Chen, Q.-W.; Zhuang, C.; Tang, P.-P.; Lin, N.; Wei, L.-Q. Controlled Release of Drug Molecules in Metal–Organic Framework Material HKUST-1. *Innorg Chem Commun* **2017**, *79*, 78–81. https://doi.org/10.1016/j.inoche.2017.03.027.

(13)

Abdouss, M.; Sharifi-sanjani, N. Oxidation of Polypropylene Homopolymer in Presence of an Aqueous Solution of Phenyltrimethyl Ammonium Permanganate. 1997.

(14)

Umemura, A.; Diring, S.; Furukawa, S.; Uehara, H.; Tsuruoka, T.; Kitagawa, S. Morphology Design of Porous Coordination Polymer Crystals by Coordination Modulation. *J. Am. Chem. Soc.* 2011, *133* (39), 15506–15513. https://doi.org/10.1021/ja204233q.

(15)

Bahrani, S.; Hashemi, S. A.; Mousavi, S. M.; Azhdari, R. Zinc-Based Metal Organic Frameworks as Nontoxic and Biodegradable Platforms for Biomedical Applications: Review Study. *Drug Metab Rev* **2019**, *51*. https://doi.org/10.1080/03602532.2019.1632887.

(16)

Crisponi, G.; Nurchi, V. M. Metal Ion Toxicity. In *Encyclopedia of Inorganic and Bioinorganic Chemistry*; Scott, R. A., Ed.; John Wiley & Sons, Ltd: Chichester, UK, 2015; pp 1–14. https://doi.org/10.1002/9781119951438.eibc0126.pub2.

(17)

Wang, K.; Yin, Y.; Li, C.; Geng, Z.; Wang, Z. Facile Synthesis of Zinc(II)-Carboxylate Coordination Polymer Particles and Their Luminescent, Biocompatible and Antibacterial Properties. *CrystEngComm* **2011**, *13* (20), 6231–6236. https://doi.org/10.1039/C1CE05705G.

(18)

Singh, D. K.; Gulati, K.; Ray, A. Effects of Chelidonic Acid, a Secondary Plant Metabolite, on Mast Cell Degranulation and Adaptive Immunity in Rats. *Int Immunopharmacol* **2016**, *40*, 229–234. https://doi.org/10.1016/j.intimp.2016.08.009.

(19)

Valgas, C.; Souza, S. M. de; Smânia, E. F. A.; Smânia Jr., A. Screening Methods to Determine Antibacterial Activity of Natural Products. *Braz. J. Microbiol.* **2007**, *38* (2), 369–380. https://doi.org/10.1590/S1517-83822007000200034.

(20)

Bernatová, S.; Samek, O.; Pilát, Z.; Šerý, M.; Ježek, J.; Jákl, P.; Šiler, M.; Krzyžánek, V.; Zemánek, P.; Holá, V.; Dvořáčková, M.; Růžička, F. Following the Mechanisms of Bacteriostatic versus Bactericidal Action Using Raman Spectroscopy. *Molecules* **2013**, *18* (11), 13188–13199. https://doi.org/10.3390/molecules181113188.

(21)

Balouiri, M.; Sadiki, M.; Ibnsouda, S. K. Methods for in Vitro Evaluating Antimicrobial Activity: A Review. *J Pharm Anal* **2016**, *6* (2), 71–79. https://doi.org/10.1016/j.jpha.2015.11.005.

(22)

Zhao, Y.; Wei, Y.; Lyu, L.; Hou, Q.; Caro, J.; Wang, H. Flexible Polypropylene-Supported ZIF-8 Membranes for Highly Efficient Propene/Propane Separation. *J. Am. Chem. Soc.* **2020**, *142* (50), 20915–20919. https://doi.org/10.1021/jacs.0c07481.

(23)

IR Spectrum Table https://www.sigmaaldrich.com/US/en/technical-documents/technical-article/analytical-chemistry/photometry-and-reflectometry/ir-spectrum-table (accessed 2022 -04 -25).

(24)

Behera, B.; Das, P. K. Blue- and Red-Shifting Hydrogen Bonding: A Gas Phase FTIR and Ab Initio Study of RR′CO···DCCl3 and RR′S···DCCl3 Complexes. *J. Phys. Chem. A* **2018**, *122* (18), 4481–4489. https://doi.org/10.1021/acs.jpca.7b11962.

(25)

Jaganyi, D.; Altaf, M.; Wekesa, I. Synthesis and Characterization of Whisker-Shaped MnO2 Nanostructure at Room Temperature. *Appl Nanosci* **2013**, *3* (4), 329–333. https://doi.org/10.1007/s13204-012-0135-3.